Available online at www.derpharmachemica.com

Scholars Research Library

Der Pharma Chemica, 2010, 2(6): 171-182
(http://derpharmachemica.com/archive.html)

ISSN 0975-413X

Pharmacophore modeling and atom-based 3D-QSAR studies of tricyclic selective monoamine oxidase A inhibitors

Mugdha R. Suryawanshi, Vithal M. Kulkarni, Kakasaheb R. Mahadik, Sharad H. Bhosale*

Department of Pharmaceutical Chemistry, Bharati Vidyapeeth Deemed University, Poona College of Pharmacy, Pune-411038, Maharastra, India

ABSTRACT

The application of first generation nonselective MAO-A inhibitors has been diminished because of their severe side effects however lately selective MOA-A inhibitors are being developed for the treatment of depression. A series of tricyclic[6,5,6]/[6,6,6] compounds have been reported as selective MOA-A inhibitors. In order to understand the structural requirement of these MAO–A inhibitors a ligand based pharmacophore and atom-based 3D-QSAR model have been developed. A four-point pharmacophore has been generated with three hydrogen bond acceptors (A) and one aromatic ring(R) denoted as A_1, A_2, A_3, and R_8. The atom based 3D-QSAR model was generated with good predictability (q^2= 0.6229) as well as fitness (r^2= 0.9595). The results of ligand-based pharmacophore hypothesis and atom based 3D-QSAR give detailed structural insights as well as highlights important binding features of tricyclic derivatives as selective MAO-A inhibitors.

Keywords: PHASE, Ligand based pharmacophore, Atom based 3D-QSAR, Selective MAO-A inhibitors

INTRODUCTION

Monoamine oxidase (MAO) is a FAD-containing enzyme of the outer mitochondrial membrane and exists as two isomezyme forms MAO-A and MAO-B. They are responsible for oxidative deamination of major neurotransmitter monoamines in the central nervous system and peripheral tissues [1, 2]. MAO-A preferably catalyzes the oxidative deamination of serotonin, adrenaline and noradrenaline and is selectively inhibited by moclobemide and clorgylene. On the other hand MAO-B selectively catalyzes the oxidative deamination of β-phenylamine and benzylamine and is selectively inhibited by selegiline. The MAO inhibitors are used for the treatment of psychiatric and neurological disorders [3,4]. Since they are involved in the metabolism of neurotransmitters they provide a good target for the design of antidepressant and anti-parkinsonian drugs [5]. Depression is a common but serious illness characterized by persistent

feelings of sadness, hopelessness, pessimism, guilt, loss of interest in activities and decreased energy. Combination of these along with many other symptoms severely affects person's professional, social and family life [6]. Most of the antidepressant drugs act by modulation of synaptic transmission of monoamines [7]. Iproniazid and tranylcipromine , the prototype of MAO inhibitors were introduced in early sixties.

They are irreversible and nonselective inhibitors [8] but found responsible for some side effects including side reactions with other drugs and food. Because of side effects the application of these first generation MAO inhibitors has been diminished. [9,10] Further research on the development of more reversible , selective and safe MAO inhibitors led to toloxatone[11].

Unlike conventional tricyclic inhibitors such as imipramine, amytryptine with heptoatomic central ring and which are nonselective MAO inhibitors with variety of side effects ; new tricyclics with pentatomic and hexatomic central ring with at least one heteroatom are being developed as selective MAO-A inhibitor [12-14].

Since last few years pharmacophore modeling has been one of the important and successful approach for new drug discovery [15-17]. A pharmacophore is concept in rational drug design that underlies the importance of specific molecular features that favor the interaction with a particular enzyme or receptor active sight[15]. A pharmacophore hypothesis can be used to know the characteristics of the binding site. For a set of active molecules, pharmacophore methods involve analyzing the molecules to identify pharmacophoric features like atoms or functional groups that can potentially interact with atoms in the binding site and then aligning the active conformations of the molecules such that their corresponding pharmacophoric features are overlaid. [15–17].

PHASE, Pharmacophore Alignment and Scoring Engine (PHASE) [18] is a comprehensive, self-contained system for pharmacophore perception, 3D-QSAR model development, and 3D database screening. PHASE uses a range of scoring techniques and fine-grained conformational sampling to generate and identify common pharmacophore hypothesis, which convey characteristics of 3-D chemical structures that are essential for binding. Each hypothesis is accompanied by a set of aligned conformations that suggest the relative manner in which the molecules are likely to bind to the receptor. Generated hypothesis with the aligned conformations may be combined with known activity data to create a 3D-QSAR model that identifies overall aspects of molecular structure that govern activity.

In the present study, ligand-based pharmacophore hypothesis and an atom-based three-dimensional quantitative structure activity relationship (3D-QSAR) is performed with for series of tricyclic[6,5,6] and tricyclic[6,6,6] compounds [12-14] as selective MAO-A inhibitors. The objective of the present study is to develop ligand-based pharmacophore hypothesis and to derive atom-based 3D-QSAR model to update the designed process for new tricyclic selective MAO-A inhibitors.

MATERIALS AND METHODS

Pharmacophore modeling

Pharmacophore modeling was carried out in Maestro 9.0 (Schrödinger ltd) [19]. A set of 65 tricyclic[6,5,6] / [6,6,6] analogs synthesized and evaluated by Harfenist et.al [12-14] as selective MAO-A inhibitors (**Table 1,2,3,4,5,6,7**) with available IC_{50} data was taken from literature for the development of ligand-based pharmacophore hypothesis and atom-based 3D-QSAR model .

The biological activity data was reported as IC_{50} (µM) and was converted to 1/Log IC_{50} (pIC_{50}) in moles to get the linearity. The dataset consists of some highly active and inactive molecules. From the total 65 compounds, 52 were randomly chosen for training set and 13 were selected as test set (**Table 1,2,3,4,5,6,7**), by using the "Automated Random Selection" option present in the PHASE software.

Generation of common pharmacophore hypothesis

The 3D structure of each compound was built using Build module with the default maestro settings. The 3D structures were minimized by default universal force field within maestro. The pharmacophore generation and atom based 3D-QSAR were performed using the PHASE module. PHASE is a versatile product of Schrödinger for pharmacophore perception, structure alignment, activity prediction, and 3D database searching. Given a set of molecules with affinity for a particular target, PHASE utilizes fine-grained conformational sampling and a range of scoring techniques to identify common pharmacophore hypothesis, which convey characteristics of 3D chemical structures that are reported to be critical for binding. Each hypothesis is accompanied by a set of aligned conformations that suggests the relative manner in which the molecules are likely to bind to the receptor. A given hypothesis may be combined with known activity data to create a 3D-QSAR model that identifies overall aspect of molecular structure that govern activity. The pharmacophore model was developed using a set of pharmacophore features to generate sites for all the compounds. Each structure is represented by a set of points in 3D space, which coincides with various chemical features that may make easy non-covalent binding among the ligand and its binding pocket [20]. PHASE provides a standard set of six pharmacophore features, hydrogen bond acceptor (A), hydrogen bond donor (D), hydrophobic group (H), negatively ionizable (N), positively ionizable (P), and aromatic ring (R).[21]

Initially conformational space of all the molecules was explored through combination of Monte-Carlo Multiple Minimum (MCMM) / Low Mode (LMOD) with maximum number of conformers 2500 per structure and minimization steps 100 [22]. Each minimized conformer was filtered through a relative energy window of 50 kJ/mol. by through sampling and redundancy check of 2Å in the heavy atom positions. Active compounds are normally considered during common pharmacophore hypothesis generation and thus pharmaset was defined by setting threshold for actives of $pIC_{50} \geq 0.65$ and a threshold for inactives of $pIC_{50} \leq 0.34$. The above mentioned pharmacophore features were introduced in all conformations by pharmacophore create site. Four point common pharmacophore hypotheses were identified from all conformation of the active ligands having identical set of features with very similar spatial arrangement keeping minimum intersite distance 2.0 A^0 in a final box size of 2.0 A^0. These common pharmacophore hypotheses were examined using a scoring function to yield the best alignment of the active ligands using an overall maximum root mean square deviation (RMSD) value of 1.2Å with default options for distance tolerance.

The quality of alignment was measured by a survival score, defined as:

$$S = WsiteSsite + WvecSvec + WvolSvol + WselSsel + W^{m}rew,$$

Where W are weights and S are scores; Ssite represents alignment score, the RMSD in the site point position; Svec represents vector score, and averages the cosine of the angles formed by corresponding pairs of vector features in aligned structures; Svol represents volume score based on overlap of van der waals models of non-hydrogen atoms in each pair of structures; and Ssel represents selectivity score, and accounts for what fraction of molecules are likely to match the hypothesis regardless of their activity toward the receptor. Wsite, Wvec, Wvol, and $W^{m}rew$ have

default values of 1.0, while Wsel has a default value of 0.0. In hypothesis generation, default values have been used. W^{m}rew represents reward weights defined by $m - 1$, where m is the number of actives that match the hypothesis. Common pharmacophore was examined, and a scoring procedure was applied to identify the pharmacophore from each box that yielded the best alignment of the active ligands. The scoring procedure provided a ranking of different hypothesis from which further investigation was carried out for appropriate hypothesis with rational choice. The hypotheses were ranked according to survival values for active and inactive compounds. The phamacophoric features involved in hypothesis were increased by two factor for active scoring.

An atom-based 3D-QSAR model is more useful in explaining the structure activity relationship than Pharmacophore-based 3D-QSAR as latter do not consider ligand features beyond the pharmacophore model. In atom-based 3D-QSAR, a molecule is treated as a set of overlapping van der Waals spheres. Each categories according to a simple set of rules: hydrogens attached to polar atoms are classified as hydrogen bond donors (D); carbons, halogens, and C–H hydrogens are classified as hydrophobic/non-polar (H); atoms with an explicit negative ionic charge are classified as negative ionic (N); atoms with an explicit positive ionic charge are classified as positive ionic (P); non-ionic atoms are classified as electron withdrawing (W); and all other types of atoms are classified as miscellaneous (X). For purposes of 3D-QSAR development, van der Waals models of the aligned training set molecules were placed in a regular grid of cubes, with each cube allotted zero or more 'bits' to account for the different types of atoms in the training set that occupy the cube. This representation gives rise to binary-valued occupation patterns that can be used as independent variables to create partial least-squares (PLS) 3D-QSAR models. Atom-based 3D-QSAR models were generated for all hypotheses using the 52-member training set using a grid spacing of 1.0Å. The best 3D-QSAR model was validated by predicting activities of the 13 test set compounds. 3D-QSAR models containing one to nine PLS factors were generated, and the models were validated by predicting the activity of test set ligands. The 3D-QSAR was evaluated by cross validated correlation coefficient (r^2_{cv}), standard error of estimation (s), Fisher test (F), correlation coefficient (r^2), Person (R). The predicted pIC_{50} are tabulated in **Tables 1,2,3,4,5,6,7**. The correlation graph between predicted and actual pIC_{50} of both training and test set are depicted in **Figure 3**. .

Table 1: In vitro MAO-A inhibitory activity of compound 1-7

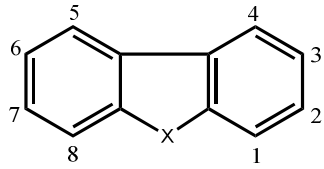

Comp	X	2	3	7	IC_{50} (µM)	Experimental pIC_{50} (M)	Predicted pIC_{50} (M)	Residual
1	O	NHAc			0.3	0.40	0.41	-0.006
2	C=O	NHAc			0.04	0.62	0.61	0.014
3^{i}	C=O	NHAc		NO_2	1.3	0.32	0.36	-0.039
$4^{t, i}$	SO_2		NH_2		1.0	0.33	0.04	0.293
5^{i}	SO_2		NHCHO		1.0	0.33	0.37	-0.037
6^{t}	SO_2		NHAc		0.26	0.41	0.41	0.004
7^{i}	SO_2		NHCOEt		1.2	0.32	0.35	-0.025

Table 2: In vitro MAO-A inhibitory activity of compound 8-14

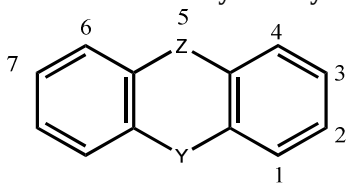

Comp	Z	Y	2	3	7	IC_{50} (µM)	Experimental pIC_{50} (M)	Predicted pIC_{50} (M)	Residual
8[t]	SO_2	C=O	NHAc			0.12	0.48	0.38	0.101
9	SO_2	C=O		NHAc		0.06	0.56	0.49	0.072
10	SO_2	C=O		NHAc	Me	0.7	0.35	0.45	-0.099
11[t,a]	SO_2	C=O		NHAc	Et	0.01	1.00	0.61	0.39
12[a]	SO_2	C=O		NHAc	Pr	0.02	0.77	0.74	0.029
13[a]	SO_2	O		NHAc		0.014	0.87	0.82	0.053
14	C=O	C=O	NHAc			0.16	0.45	0.39	0.064

Table 3: In vitro MAO-A inhibitory activity of compound 15-28

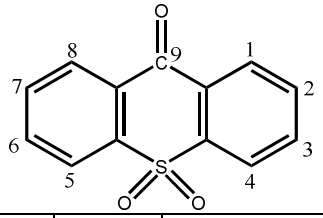

Comp	Substituent	IC_{50} (µM)	Experimental pIC_{50} (M)	Predicted pIC_{50} (M)	Residual
15[i]	2-Br	1.0	0.33	0.52	-0.187
16	3-CONHMe	0.06	0.56	0.71	-0.148
17[t]	2,6-$(CONHMe)_2$	0.05	0.58	0.72	-0.131
18	5-Me-3-CONHMe	0.05	0.59	0.63	-0.041
19[a]	7-Me-3-CONHMe	0.008	1.07	0.92	0.187
20	7-*i*-Pr-3-$CONH_2$	0.7	0.35	0.6	-0.249
21[a]	7-*i*-Pr-3-CONHMe	0.006	1.28	1.04	0.245
22	7-PrO-3- $CONH_2$	0.45	0.38	0.45	-0.073
23[a]	7-PrO-3- CONHMe	0.002	0.32	0.39	-0.068
24	7-OAc-3-CONHMe	0.13	0.47	0.42	0.053
25	7-OCH_2COOMe-3-CONHMe	0.3	0.40	0.26	0.144
26[a]	7-NMe_2-3-CONHMe	0.03	0.68	0.76	-0.083
27[t,a]	5,7-Me_2-3-CONHMe	0.02	0.77	0.74	0.029
28	3-C(=NH)NHMe	0.06	0.56	0.35	0.212

Table 4: In vitro MAO-A inhibitory activity of compound 29-36

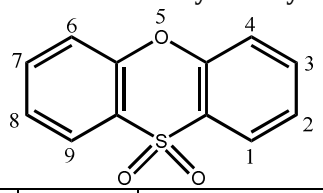

Comp	Substituent	IC_{50} (µM)	Experimental pIC_{50} (M)	Predicted pIC_{50} (M)	Residual
29	----	0.05	0.59	0.52	0.069
30	2-CN	0.2	0.43	0.42	0.015
31[a]	2-CONHMe	0.03	0.68	0.64	0.037
32	3-CN	0.06	0.56	0.55	0.012
33[t]	3-CONHMe	0.6	0.36	0.37	-0.01
34	3-$C(O)NHC_2H_4NHAc$	0.3	0.40	0.45	-0.046
35	2-OCONHMe	0.2	0.43	0.44	-0.005
36	2,7-DiAc	0.5	0.37	0.42	-0.049

Table 5: In vitro MAO-A inhibitory activity of compound 37-38

Comp	Structure	IC_{50} (µM)	Experimental pIC_{50} (M)	Predicted pIC_{50} (M)	Residual
37	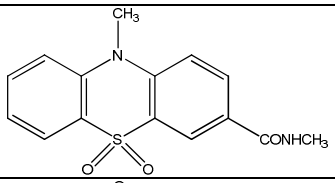	0.3	0.40	0.41	-0.006
38	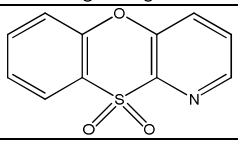	0.6	0.36	0.37	-0.01

Table 6: *In vitro* MAO- A inhibitory activity of compound 39-61

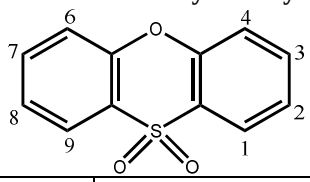

Comp	Substituent	IC_{50} (µM)	Experimental pIC_{50} (M)	Predicted pIC_{50} (M)	Residual
39[a]	1-Me	0.03	0.68	0.59	0.087
40	3-Me	0.2	0.43	0.54	-0.105
41	4-Me	0.8	0.34	0.35	-0.006
42	1-Et	0.07	0.54	0.53	0.012
43[a]	2-Et	0.007	1.18	1.03	0.153
44[t,a]	3-Et	0.006	1.29	1.36	-0.274
45[i]	4-Et	1.0	0.33	0.37	-0.037
46	1-CH=CH_2	0.04	0.62	0.58	0.044
47	1-C≡CH_2	0.1	0.50	0.57	-0.07
48[t]	1-CF_3	0.08	0.52	0.58	-0.054
49	1-CH_2OH	0.14	0.46	0.47	-0.004
50[a]	1-CH_2CH_2OH	0.02	0.77	0.77	-0.001
51[i]	2-C(O)Me	1.0	0.33	0.41	-0.077
52	1-C(O)COOMe	0.6	0.36	0.39	-0.03
53	1-CH_2Br	0.1	0.50	0.52	-0.02
54[t]	2-OMe	0.2	0.43	0.52	-0.085
55	2-OEt	0.04	0.62	0.69	-0.066
56	1-Br	0.06	0.56	0.55	0.012
57[a]	3-Br	0.02	0.76	0.77	-0.001
58	1-I	0.05	0.59	0.57	0.019
59[t]	1,9-Me_2	0.05	0.59	0.62	-0.031
60	1-Et-7-OH	0.11	0.49	0.5	-0.01
61	1-Et-2-OMe	0.6	0.36	0.34	0.02

Table 7: In vitro MAO-A inhibitory activity of compound 62-65

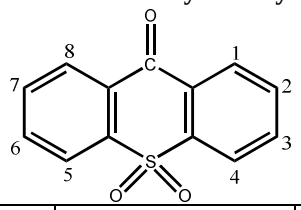

Comp	Substituent	IC_{50} (µM)	Experimental pIC_{50} (M)	Predicted pIC_{50} (M)	Residual
62	4-Me	0.06	0.56	0.35	0.212
63	4-Et	0.4	0.38	0.36	0.024
64	4,5-Me_2	0.3	0.40	0.38	0.024
$65^{t,i}$	2-Br	1.0	0.33	0.51	-0.177

a = active pharmaset, i= inactive pharmaset, t = test set.

Table 8: Best Pharmacophore hypothesis according to scoring values

Hypothesis	Survival Active	Survival Inactive	Post-hoc	#Matches
AARR.1	7.280	4.859	3.708	14
AARR.2	7.173	4.721	3.602	14
AARR.4	7.173	4.721	3.602	14
AARR.5	7.173	4.721	3.602	14
AARR.3	7.173	4.721	3.602	14
AARR.6	6.987	5.155	3.401	14
AAAR.31	6.875	4.847	3.409	14
AAAR.22	**6.875**	**4.847**	**3.409**	**14**
AAAR.10	6.875	4.847	3.409	14
AARR.10	6.863	5.055	3.287	14
AARR.8	6.863	5.055	3.287	14
AARR.7	6.863	5.055	3.287	14
AARR.9	6.863	5.055	3.287	14
AAAR.4	6.843	4.675	3.401	14
AAAR.7	6.843	4.675	3.401	14
AAAR.19	6.843	4.675	3.401	14
AAAR.5	6.738	4.609	3.297	14
AAAR.6	6.738	4.609	3.297	14
AAAR.20	6.738	4.609	3.297	14
AAR.21	6.738	4.609	3.297	14

Table 9: Statistic parameters for best pharmacophore hypothesis

PLS Factors	SD	r^2	F	P	RMSE	q^2	Pearson-R
1	0.3982	0.2047	12.9	0.0007574	0.7206	0.114	0.3089
2	0.2998	0.5581	30.9	2.042e-009	0.1724	-0.2439	0.4693
3	0.2016	0.8043	65.8	5.049e-017	-0.0485	-0.0185	0.6006
4	0.1572	08835	89.1	2.514e-021	-0.0749	0.3528	0.7038
5	0.1203	0.9332	128.6	7.473e-026	-0.0976	0.5954	0.811
6	**0.0951**	**0.9592**	**176.1**	**7.473e-029**	**-0.117**	**0.6229**	**0.838**
7	0.0766	0.9742	236.5	1.496e-033	-0.1303	0.593	0.8327
8	0.0662	0.9811	279.3	1.753e-034	-0.1301	0.587	0.8309
9	0.0576	0.986	329	5.678e-036	-0.1333	0.5811	0.8316

Figure 1: Pharmacophore hypothesis and distance between pharmacophoric sites, all distances are in A^0 unit

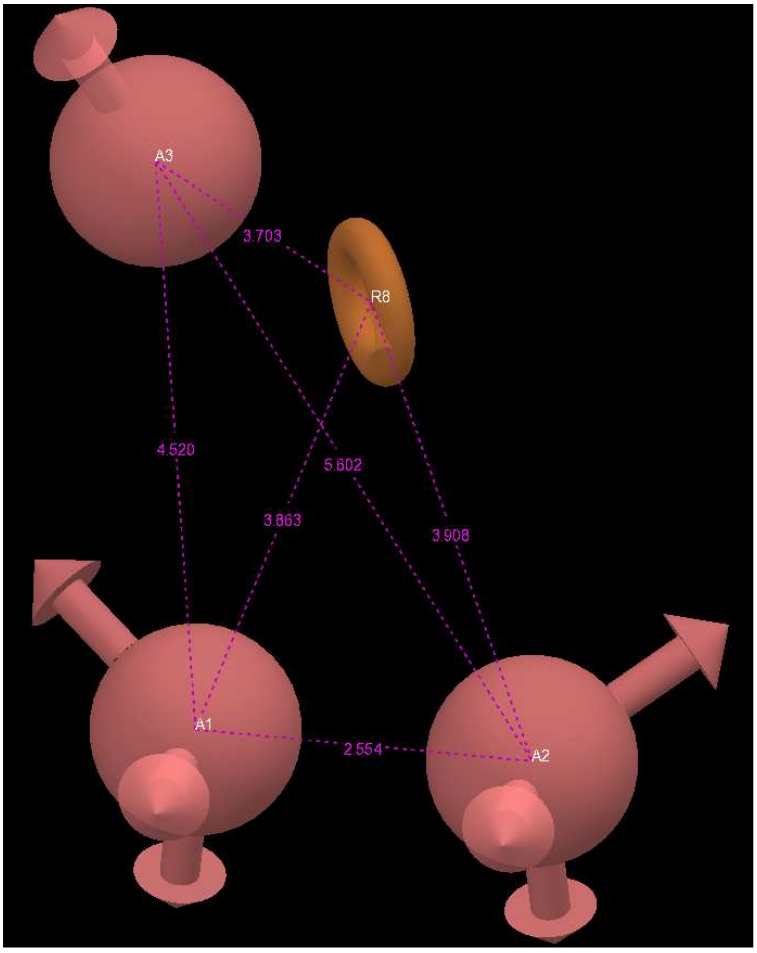

Figure 2: Pharmacophore hypothesis aligned on the reference ligand 19

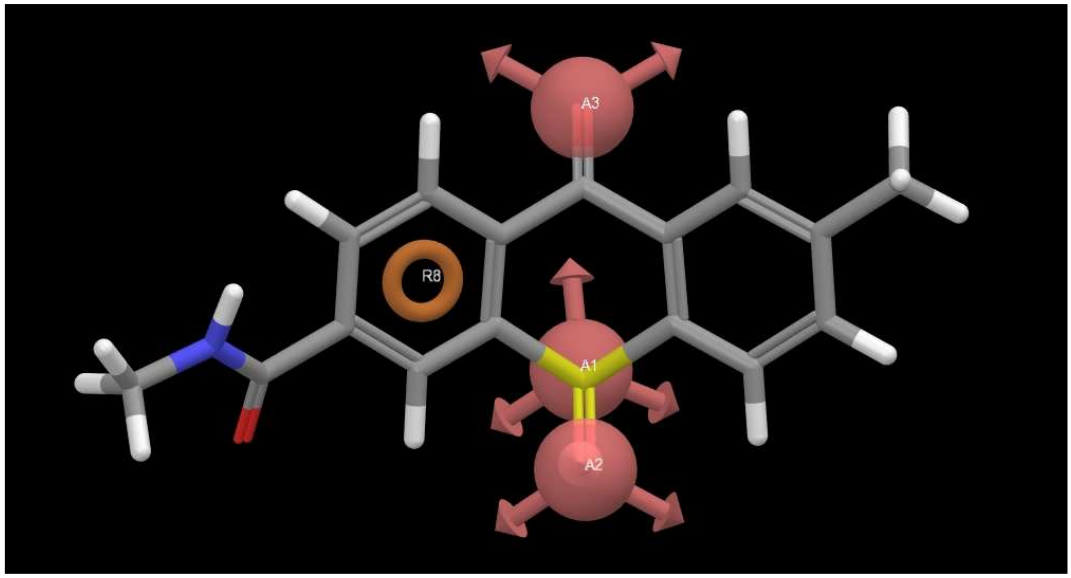

Figure 3: Correlation graph of Experimental versus predicted pIC_{50} of training (a) and test sets (b)

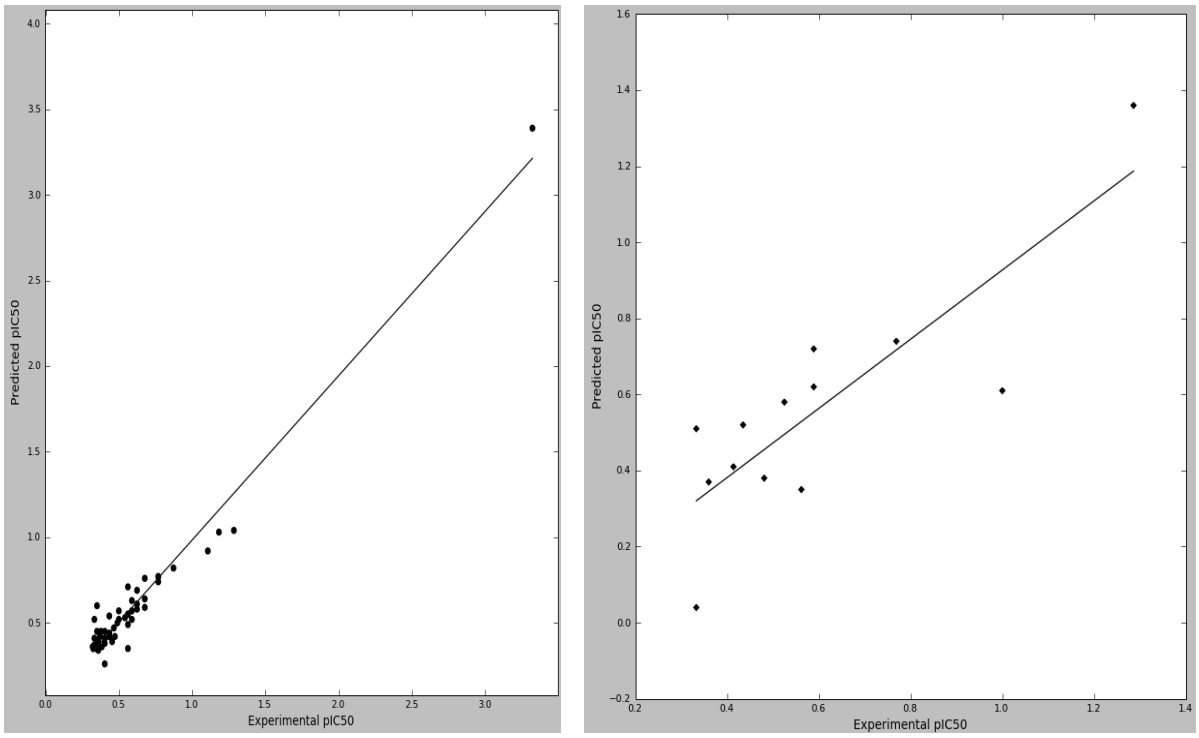

(a) **(b)**

Figure 4: Visual representation of atom-based 3D-QSAR on most active ligand 23

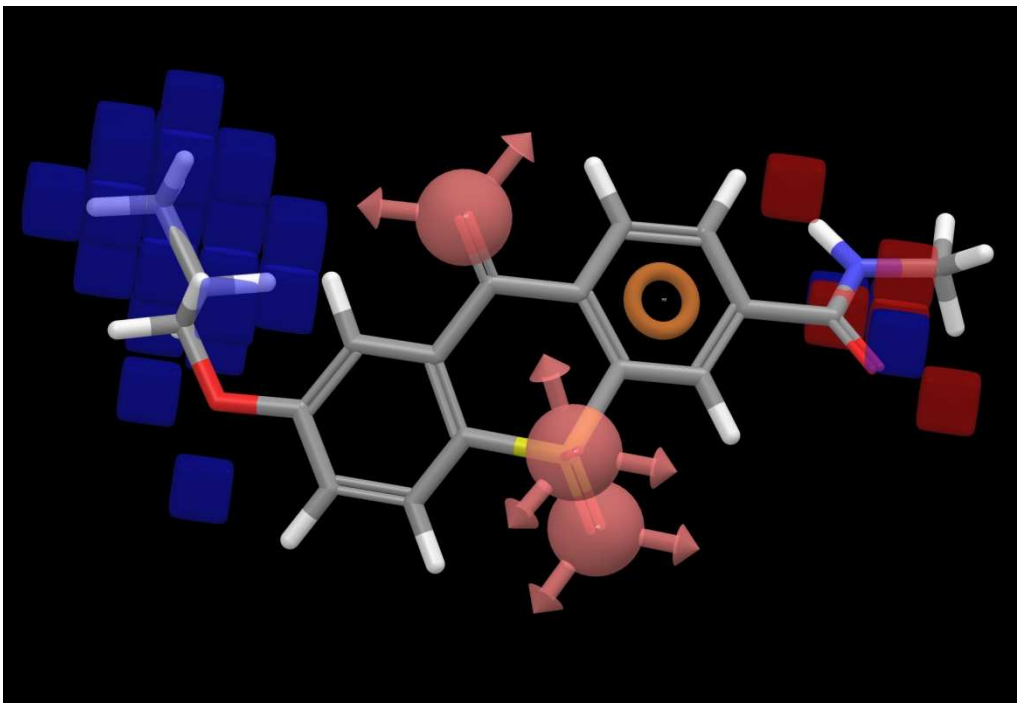

Figure 5: Visual representation of atom-based 3D-QSAR on least active ligand 3

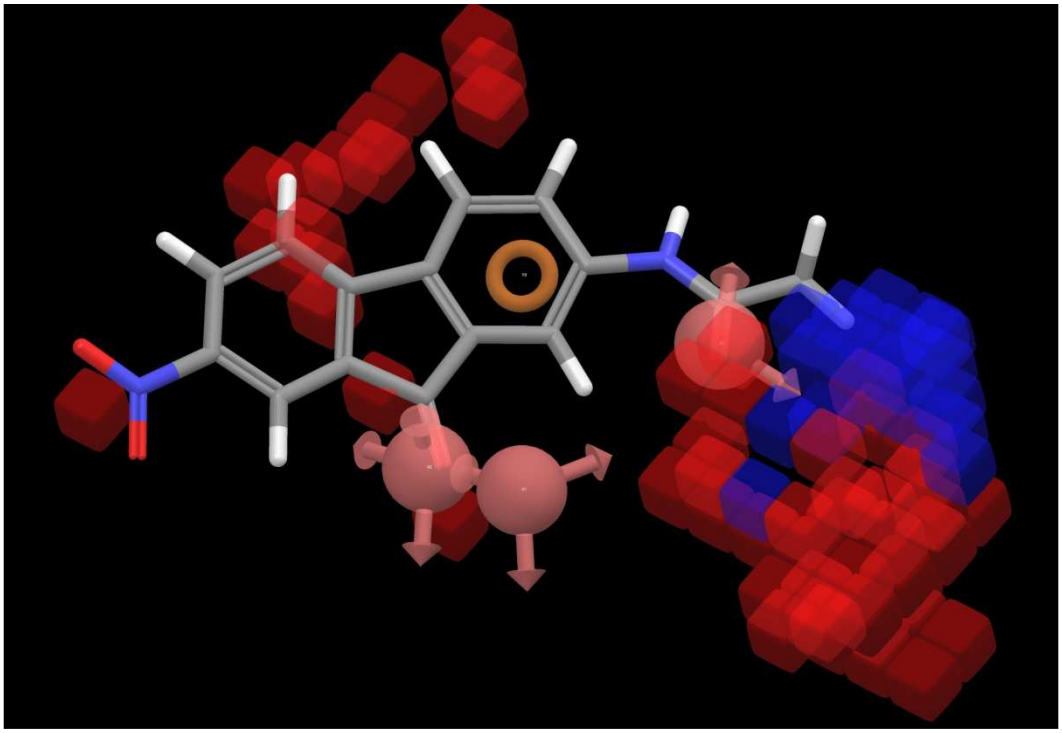

RESULTS AND DISCUSSION

After completion of common pharmacophore we were able to identify a total of 20 different hypotheses (**Table 8**). The best model was found to be associated with four-point hypothesis (**Figure 1**), which consists of three hydrogen bond acceptors (A) and one aromatic ring(R) denoted as A_1, A_2, A_3, and R_8. The pharmacophore hypothesis aligned on reference ligand **16** is depicted in **Figure 2**. Pharmacophore sites spatial distribution of AAAR. 22 models show three acceptor sites intercalated by a aromatic site in a tetrahedral space of about 4 A^0. The three hydrogen bond acceptor A_1, A_2 and A_3 form scalene triangle. The distances between A_1- A_2, A_1-$A_3$and A_2-A_3 are 2.554, 4.520 and 5.602 A^0 respectively. The aromatic ring (R_8) is slightly orientated towards the site A_1.

For the 3D-QSAR models generation, non-modeled (inactive or moderately active) molecules in the dataset were then aligned on the basis of their matching with at least four pharmacophore features. The pharmacophore hypothesis yielded a 3D-QSAR model with good PLS statistics. The 3D-QSAR was evaluated by cross validated correlation coefficient (r^2_{cv}), standard error of estimation (s), Fisher test (F), correlation coefficient (r^2) and Pearson-R. The predicted pIC_{50} are tabulated in **Tables 1,2,3,4,5,6,7.** The goodness of the model was validated by q^2 for test set (**Table 9**).The training set correlation is characterized by PLS factor **6** (r^2 = 0.9592, SD=0.0951,F =176.1 Pearson-R =7.437e−29). The test set correlation is characterized by PLS factors 6 (q^2 =0.6229, RMSE=-0.117, Pearson-R =0.838). Results of PLS statistics of atom-based 3D-QSAR are shown in **Table 8**. Correlation graph of Experimental versus predicted pIC_{50} of training and test sets are shown in **Figure 3**. Additional insights into the inhibitory activity can be gained by visualizing the 3D-QSAR model in the context of one or more ligands in the series with diverse activity. A pictorial representation of the cubes generated in the present 3D-QSAR for most active ligand **44** and least active ligand **3** is shown in **Figure 4** and **5** respectively. In these

generated cubes, the blue cubes indicate favorable features, while red cubes indicate unfavorable features for biological activity.

The blue cubes around aromatic C_7 of the most active compound **23** suggest that substitution at C_7 aromatic carbon is favorble for biological activity. Further substitution with aliphatic chain at C_7 aromatic carbon significantly increased the activity. Thus compounds having aliphatic substitution at C_7 position (compound **19**, **21**, **26**, **27**) are more active than substitution by other group at C_7 position in the ring (compound **22, 24, 25**). Moreover, the most significant favorable and unfavorable features observed at the C_3 of the aromatic ring which indicated that presence of N-methyl amide group is essential for biological activity. Therefore compounds having N-methyl amide group are more active than the compound having unsubstituted amide group.

In **Figure 6** the red cube adjacent to the nitro group of the least active compound **3** indicates that presence of polar substitution on C_7 carbon of the aromatic ring diminish the biological activity. The blue cubes around keto of the anilide group indicate that presence of anilides at C_2 position of the aromatic ring favors the biological activity relatively as seen in compound **1** and **2,** while the compounds having substitution at C_3 position of the aromatic ring in compounds **4,5,7** exhibit weak activity.

CONCLUSION

In conclusion, a highly predictive pharmacophore hypothesis was generated using a training set of 65 molecules. It is a four-point pharmacophore hypothesis with three hydrogen bond acceptors (A) and one aromatic ring (R) denoted as A_1, A_2, A_3, and R_8. An atom-based 3D-QSAR models were generated for all hypotheses using the 52-member training set. The predictive power of the atom based 3D-QSAR was well validated using 13 member of test set. The developed atom-based 3D-QSAR model can provide insights into the structural requirement of novel tricyclic [6,5,6] / [6,6,6] compounds as selective MAO- A inhibitors. The present study aimed to develop ligand-based pharmacophore hypothesis and atom-based 3D-QSAR gives detailed structural insights as well as highlights important binding features of tricyclic derivatives as selective MAO-A inhibitors, which can provide guidance for the rational design of novel potent selective MAO-A inhibitors.

REFERENCES

[1] Bach, AW, Lan, NC, Johnson, DL, Abell, CW, Bembeneck, ME, Kwan, SW. Seeburg, PH. and Shih, JH, *Proc. Natl. Acad. Sci. USA*, **1988**, 85, 4934–4938.
[2] Shih, J. C.; Chen, K.; Ridd, M. J. *Annul. Rev. Neurosci*., **1999**, *22*, 197-217.
[3] Andrews, J. M.; Nemeroff, C. B. *Am. J. Med. Chem***.,** **1994**, *97*, 24S-32S.
[4] Cesura, A. M.; Pletscher, A. *Prog. Drug Res.*, **2002**, *38*, 171-298.
[5] Checkoway, H.; Franklin, GM.; Costa-Mallen, P.; Smith-Weller,T.; Dilley, J.; Swansons, P D.; Costa LG. *Neurology*, **1998**, *50*, 1458-1461.
[6] Manual of Depression, National Institute of Health, Bethesda, **2008**, 2.
[7] Shelton, R. C. *Expert Opin. Ther. Pat.*, **2001**, *11*, 1693-1711.
[8] Ban, TA., *J. Neural Transm*., **2001**, *108*, 707-716.
[9] Blackwell, B. *Drugs*, **1981**, *21*, 201-219.
[10] Bieck, P. R.; Antonin, K.H. *American Psychiatric Press: Washington*, DC, **1994,** 83-110.
[11] Curet, O.; Damoiseau, G.; Aubin, N.; Sontag, N.; Rovei, V.; Jarreau, F.-X. Befloxatone, *J. Pharmacol. Exp. Ther.*, **1996**, *277*, 253-264.

[12] Morton Harfenist, Charles T. Joyner,Patric D. Mize and Helen L. White; *J. Med.Chem.*,**1994**, 37, 1885-2090.
[13] Morton Harfenist, Diane M. Jopseph, Sharon C. Spence, Daniel PC. Mcgee, Mark D. Reeves and Helen L. White: *J. of Med. Chem.*, **1997**, 40, 16, 2466- 2473.
[14] Morton Harfenist, Daniel P. C. Mcgee, Mark D. Reeves and Helen L. White, *J. of Med. Chem.*, **1998**, 41, 12, 2118- 2125.
[15] Marriott DP, Dougall IG, Meghani P, Liu YJ, Flower DR, *J. Med. Chem.*,**1999**, 42, 3210–3216.
[16] Talele TT, Kulkarni SS, Kulkarni VM, *J. Chem. Comput. Sci.*, **1999** 39, 958–966.
[17] Karki RG, Kulkarni VM *Eur. J. Med. Chem.*, **2001**, 36, 147–163.
[18] Phase, version 3.1, Schrödinger, LLC, New York, USA, **2009**.
[19] Maestro, version 9.0, Schrödinger, LLC, New York, USA, **2009**.
[20] Dixon SL, Smondyrev AM, Knoll EH, Rao SN, Shaw DE, *J. Comput. Aided Mol. Des.*, **2006.**
[21] Chang G, Guida WC, Still WC *J. Am. Chem. Soc.*, **1989**, 111, 4379–4386.
[22] Kolossvary I, Guida WC *J. Am. Chem. Soc.*, **1996**, 118: 5011–5019.